Computers, Materials & Continua

Tech Science Press

DOI: 10.32604/cmc.2024.047093

ARTICLE

Learning Epipolar Line Window Attention for Stereo Image Super-Resolution Reconstruction

Xue Li, Hongying Zhang*, Zixun Ye and Xiaoru Huang

School of Information Engineering, Southwest University of Science and Technology, Mianyang, 621010, China

*Corresponding Author: Hongying Zhang. Email: zhywyd@163.com

Received: 24 October 2023 Accepted: 26 December 2023 Published: 27 February 2024

ABSTRACT

Transformer-based stereo image super-resolution reconstruction (Stereo SR) methods have significantly improved image quality. However, existing methods have deficiencies in paying attention to detailed features and do not consider the offset of pixels along the epipolar lines in complementary views when integrating stereo information. To address these challenges, this paper introduces a novel epipolar line window attention stereo image super-resolution network (EWASSR). For detail feature restoration, we design a feature extractor based on Transformer and convolutional neural network (CNN), which consists of (shifted) window-based self-attention ((S)W-MSA) and feature distillation and enhancement blocks (FDEB). This combination effectively solves the problem of global image perception and local feature attention and captures more discriminative high-frequency features of the image. Furthermore, to address the problem of offset of complementary pixels in stereo images, we propose an epipolar line window attention (EWA) mechanism, which divides windows along the epipolar direction to promote efficient matching of shifted pixels, even in pixel smooth areas. More accurate pixel matching can be achieved using adjacent pixels in the window as a reference. Extensive experiments demonstrate that our EWASSR can reconstruct more realistic detailed features. Comparative quantitative results show that in the experimental results of our EWASSR on the Middlebury and Flickr1024 data sets for 2 × SR, compared with the recent network, the Peak signal-to-noise ratio (PSNR) increased by 0.37 dB and 0.34 dB, respectively.

KEYWORDS

Stereo SR; epipolar line; window attention; feature distillation

1 Introduction

Deep learning-based super-resolution reconstruction (SR) of stereo images is an important research direction in the field of computer vision, and its core idea is to utilize the information in multi-view images to infer high-resolution image information [1–3] acquire two low-resolution images using devices such as binocular cameras, then match and fuse these images to obtain high-resolution images from different viewpoints. Stereo SR has garnered increased attention in various disciplines, showcasing excellent results in competitions like the new trends in image restoration and enhancement (NTIRE) [4], demonstrating the potential of stereo correspondence information to improve SR performance. However, Stereo SR faces several challenges. Firstly, it must recover high-frequency details, including object edges and fine features, from low-resolution left and right-view images. Effectively recovering and enhancing these high-frequency features remains a major challenge. Secondly, there is the task of fusing left and right view information. Stereo SR requires the integration of information from both viewpoints to improve depth estimation accuracy, demanding an effective information fusion strategy to combine the data from both views and obtain better depth maps. Lastly, the models employed tend to have a large number of parameters. Stereo SR tasks typically necessitate deep neural network models for learning the mapping from low-resolution to high-resolution. Designing a Stereo SR model that is both efficient and lightweight is extremely challenging due to the complex structure of high-resolution depth images.

The issues above represent some of the key challenges in Stereo SR research. To restore more discriminative high-frequency features, Hui et al. [5] introduced perceptual techniques to enhance and improve the performance of super-resolution algorithms, making the reconstructed stereo images more suitable for human vision or computer vision systems, thus enhancing perceptual quality [6–8] employ non-autoregressive fusion network (NAFnet) denoising modules to handle noise interference in images, promoting the recovery of high-frequency features. To utilize complementary information between images, DASSR adopted a disparity-based domain adaptation approach to merge views, taking into consideration depth information for adapting to varying disparities. Dai et al. [9] introduced a feedback mechanism by transferring information extracted from super-resolution tasks into disparity estimation tasks, establishing a mutual feedback loop that enhances performance in both tasks. Software Architecture Evaluation Model (SAEM) [10] makes efficient use of information from both cross-view and intra-view perspectives to acquire cross-view information, thereby improving image SR performance [11–13] explored distillation, fusion, and feature enhancement to achieve model lightweight and efficiency, proposing an efficient separable distillation module for high-resolution feature restoration. References [14–16] transformed 3D or 4D cost volumes into disparity learning approaches, reducing significant computational costs. Despite substantial progress in previous research, a balance between long-range feature dependencies (perception) and local information attention remains essential for high-frequency feature recovery. Furthermore, when employing a disparity attention mechanism for complementary information fusion, particular attention should be paid to the upper and lower offsets of complementary information within the epipolar line range.

In response to the challenges posed by Stereo SR outlined above, this paper introduces a cross-view fusion attention network partitioned along the epipolar lines. First, to address issues regarding image perception and local feature attention, a Swin Transformer feature distillation and enhancement block (FDEB) Layer is introduced for global feature extraction and fine-grained local feature extraction, which utilizes a (shifted) window-based self-attention ((S)W-MSA) and a FDEB. Furthermore, adaptive overlapping window attention enhances long-range dependencies between (S)W-MSA feature pixels. Second, to effectively incorporate stereo correspondence information, we propose an epipolar line window attention (EWA) mechanism. This mechanism enables the network to learn the similarity between a pixel and the pixels within the window along its epipolar line. Moreover, partitioned window information contributes to improved pixel-matching accuracy in regions characterized by pixel smoothness. Comparative experiments on a stereo dataset show that our network has superior SR performance with fewer parameters. Our contributions can be summarized as follows:

(1) We propose the EWASSR network, which combines (S)W-MSA and FDEB to enhance the recovery of fine-grained details in Stereo SR. Experimental results demonstrate a significant improvement in SR performance with the introduction of FDEB.

(2) We introduce an EWA attention mechanism that partitions windows along the epipolar line to address pixel misalignment issues between stereo views, enabling more accurate pixel matching. Experimental results show that this model pays more attention to the discriminative features in the image after fusing stereo views through EWA.

(3)The proposed EWASSR achieves superior performance with fewer parameters than recent stereo SR methods.

2 Related Work

2.1 Single Image SR

With the development of deep neural networks, the single-image super-resolution (SISR) task based on deep learning has made significant progress [17], as shown in Fig. 1. Early SISR models [18–20] using deep learning employed multiple convolutional layers to learn image features, laying the foundation for subsequent research. Some networks [21–24] achieved better noise and artifact suppression through recursive learning. The introduction of residual networks addressed the problems of gradient vanishing and exploding during deep network training. Some networks [25–29] also utilized residual methods to deepen the depth of feature extraction, obtaining richer image semantic features. To facilitate the model's focus on more important regions in the image, references [30,31] proposed integrating attention mechanisms into the SR model. Recently, Khan et al. [32] introduced a holistic attention network to address the issues of channel attention ignoring the relevance of feature layers and modeling layer dependencies. Jiang et al. [33] tackled the challenge of comparing SISR algorithms fairly by introducing a real-world dataset and proposing a new objective metric using the Karhunen-Loéve Transform. SR3 [34] employed denoising diffusion models for image-to-image translation, demonstrating excellent super-resolution performance across diverse tasks, including faces and natural images. Addressing the interaction issues between Transformer windows, Chen et al. [35] introduced a new hybrid attention Transformer (HAT), which aggregates information between overlapping cross windows. To address the lack of multi-scale information in shift windows, SwinFIR [36] used fast Fourier convolution to make the network focus on spatial and frequency domain information, further enhancing its ability to capture global information. SRFormer [37] addressed the issue of increased computational complexity with large windows in SwinIR that improves SR performance. Park et al. [38] designed the dilated window transformer for global feature extraction. To maintain model efficiency while focusing on details, Residual Feature Distillation Network (RFDN) [39] aggregated features of different scales and edges with high-frequency information through channel distillation and enhancement, also serving as the baseline for efficient SR channels in NTIRE, solving the issue of large parameterization in SR models. While SISR excels in multi-scale feature extraction and lightweight models, it is not directly applicable to recovering high-frequency features and fusing complementary information in stereo tasks.

2.2 Stereo SR

Stereo SR enhances image quality in visual tasks, contributing to advancements in computer vision, as illustrated in Fig. 1. Jeon et al. [2] aligned left and right pixels by imposing maximum disparity priors. Some networks [5,9,40,41] achieved pixel alignment by iteratively estimating disparities between images. To address the issue of uncontrollable disparity ranges, Wang et al. [42,43] proposed a Disparity Attention Mechanism (PAM), enabling the learning of similar information along the epipolar line. PAM employs a low-cost fusion of stereo views but lacks attention to image-specific information. Therefore, Song et al. [44] combined self-attention to focus on both image-specific and cross-view information along the epipolar line. Similarly, IMSSRnet [45] notably improved stereoscopic image super-resolution by leveraging complementary information, outperforming state-of-the-art methods with gradient and disparity losses. Based on this, CPASSRnet [46] achieved single-model super-resolution with multiple scale factors in both views, addressing challenges in stereo images such as large disparities and different epipolar lines. While PAM effectively integrates complementary information in stereo images, its asymmetry prevents the network from simultaneously obtaining SR images for the left and right views. To address this, Ying et al. [47] developed a universal stereo-view attention mechanism, demonstrating excellent SR performance when applied to the SISR task. To tackle occlusion issues between stereo images, inspired by PASSRnet [42], iPASSR [48] updated the valid mask design in PAM, effectively handling occluded view information. Accurate assessment of disparity information contributes to feature complementarity in stereo image pairs. LF-DGNet [49] introduced a disparity-guided feature modulation module, a multi-view feature recalibration module, and a disparity-guided network for light field spatial super-resolution. Building on this, some networks effectively fuse complementary information in stereo images and promote Stereo SR reconstruction tasks by designing cross-view attention. NAFSSR [6] achieved outstanding SR performance by combining the stereo cross attention module (SCAM) with the denoising non-autoregressive fusion block (NAFBlock). To cut down on computational expenses, Chen et al. [50] introduced the residual cross attention module (RCAM) for fusing view information. Ying et al. [10] utilized a cross-view fusion transformer for integrating cross-view information and an intra-view refinement transformer to refine intra-view features, maximizing the use of complementary information. Although these view attention mechanisms effectively address the epipolar pixel alignment issue, the alignment of pixels shifting along the epipolar line in stereo views also requires attention. Therefore, in this work, we designed an epipolar window attention to address pixel displacement in the fusion of complementary information in stereo views.

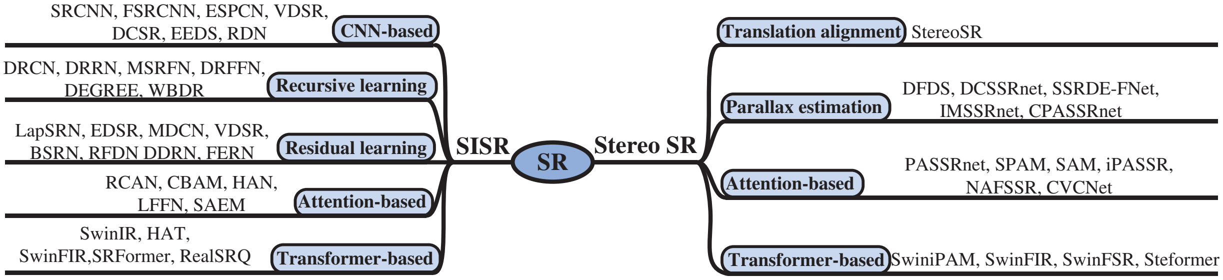

Figure 1: Classification of image super-resolution reconstruction techniques

3 Materials and Methods

3.1 Network Architecture

Given a pair of low-resolution images, L_L and L_R, our EWASSR simultaneously reconstructs the high-resolution left image S_L and right image S_R, as shown in Fig. 2. Feature extraction module is divided into shallow feature extraction and deep feature extraction. We initiate the process by employing a 3 × 3 convolutional layer for mapping the RGB space to a high-dimensional feature space. Next, we utilize the residual Swin Transformer FDEM block (RSTFB) to extract deep image features. RSTFB is inspired by the residual hybrid attention groups (RHAG) and residual Swin Transformer block (RSTB). It combines Transformer and CNN-based feature extraction techniques to progressively recover lost high-frequency features in the image. RSTFB is detailed in Section 3.2 and includes key components such as (S)W-MSA, FDEB, and overlapping cross-attention block (OCAB). Using RSTFB for feature extraction offers two significant advantages. First, Swin Transformer layer (STL) is based on the attention mechanism to realize efficient global information acquisition capability. Second, the CNN-based FDEB excels at extracting high-quality local features. Therefore, RSTFB helps address issues related to establishing long-range dependencies and capturing local detail features in the image, resulting in a diverse set of features that comprehensively describe the image content.

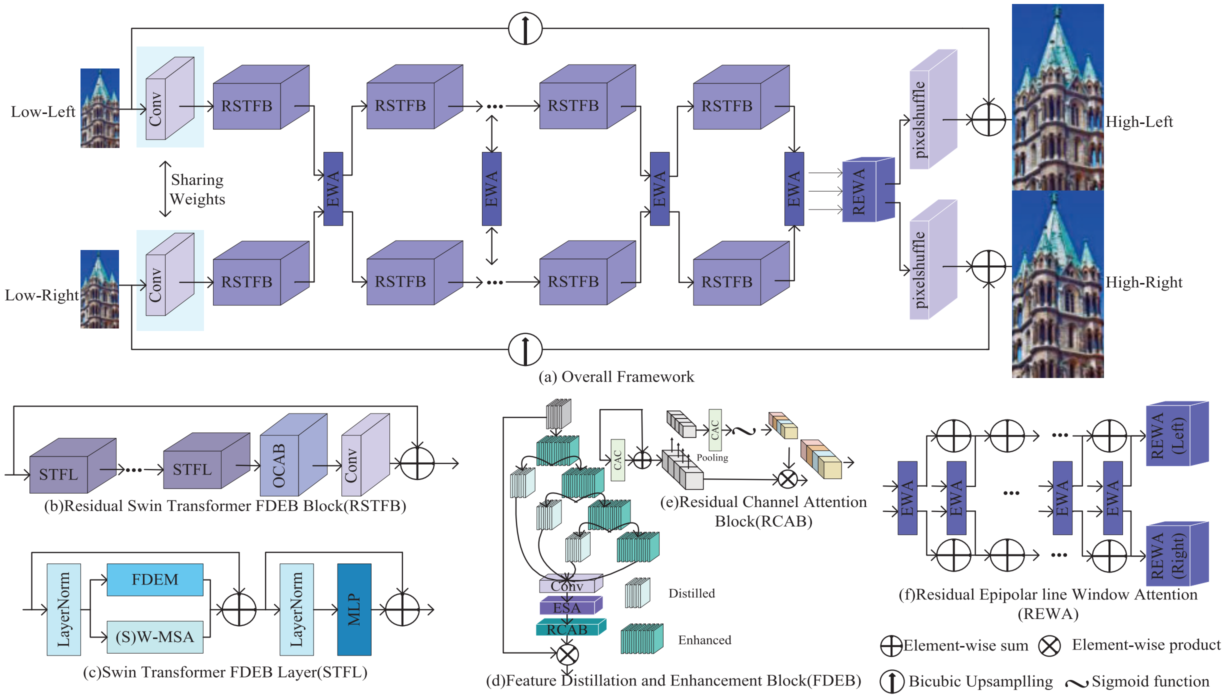

Figure 2: An overview of our EWASSR. “Conv” represents a 3 × 3 convolutional layer. “OCAB” in (b) is overlapping cross-attention block. Distilled in (d) consists of a 1 × 1 convolutional layer and GELU, and Enhanced consists of a 3 × 3 convolutional layer and GELU

Feature fusion consists of two stages. In the first stage, we employ an iterative feature fusion approach. Initially, the outputs of RSTFB are used as inputs for the epipolar line window attention (EWA), which is detailed in Section 3.4. EWA employs a novel attention network that partitions along the epipolar line windows, effectively fusing complementary information from the left and right views. Subsequently, the outputs of EWA are used as inputs for the next layer of RSTFB, which extracts semantic information from the preliminarily aligned disparity map. This process is iterated multiple times, progressively enhancing the network’s ability to learn features. In the second stage, we perform multi-level feature fusion. All the outputs of a series of EWAs from the first stage are used as inputs for the residual epipolar line window attention (REWA). This stage involves re-fusing the multi-level features, enhancing the representation capability of the disparity map features.

3.2 *Residual Swin Transformer FDEB Block (RSTFB)*

Given stereo low-resolution image inputs $L_L \in \mathbb{R}^{H\times W\times C_0}$ and $L_R \in \mathbb{R}^{H\times W\times C_0}$ (H, W and C_0 are the images’ height, width and input channel number, respectively, where $C_0 = 3$), we use a 3 × 3 convolutional layer to map the stereo images from the low-dimensional space to the high-dimensional space. Convolution is used to achieve channel conversion while extracting shallow features, which is efficient and concise [34]. For deep features, As shown in Fig. 2b, RSTFB is a residual block with Swin Transformer FDEB layers (STFLs), an OCAB and a convolutional layer. Take the first layer RSFTB for example, given a stereo input image pair $F_L \in \mathbb{R}^{H \times W \times C_1}$ and $F_R \in \mathbb{R}^{H \times W \times C_1}$ (where $C_I = 96$), the image multi-scale features are first extracted after i (where $i = 6$ is following [33,34]) STFLs, an OCAB and a 1×1 convolutional layer to obtain the feature tensor $F_L^j \in \mathbb{R}^{H \times W \times C_1}$ and $F_R^j \in \mathbb{R}^{H \times W \times C_1}$ as:

$$\begin{cases} F_L^j = Conv\_1\left(OCAB\left(iSTFLs\left(F_L\right)\right)\right) \\ F_R^j = Conv\_1\left(OCAB\left(iSTFLs\left(F_L\right)\right)\right) \end{cases}, \tag{1}$$

where j represents the j-th RSTFB, we have defined $j = 1, 2, \ldots, 8$. OCAB refers to the overlapping cross-attention block. Inspired by HAT, we use an overlap ratio $r = 2/M$ to adapt to different overlapping areas of the windows. The size of the overlapping window M_0 is obtained by increasing the length and width of the original window M by 1. This design ensures that overlapping pixels are constrained within an adaptive range, preventing them from growing indefinitely as the window size increases and thus avoiding redundant computation of interaction information in large windows. STFL consists of (S) W-MSA and FDEB operations. A detailed description of FDEB can be found in Section 3.3. Our EWASSR improves upon previous work by employing a more concise and efficient method of cascading feature extraction and fusion alternately, significantly reducing the number of model parameters compared to the previous approach of concatenating deep feature extraction modules in series.

3.3 *Feature Distillation and Enhancement Block (FDEM)*

FDEB is based on feature distillation network [12,39]. As shown in Fig. 2d. We first increase the dimension of the input feature channels to twice the original number of channels. The channel enhancement operation increases the focus on image edges or textures, enhancing the model's ability to capture object motion trajectories and edge information. Channel distillation reduces the dimension of feature channels to half the number of enhanced channels, enabling the network to learn more discriminative features. Its purpose is to aid the network in better understanding the image content by transmitting clear image features. Given intermediate feature maps, the operations of FDEB are as follows:

$$\begin{cases} F_L^{out} = RCAB\left(ESA\left(Conv\_3\left(Cat\left(F_L^{D1}, F_L^{D2}, F_L^{D3}, F_L^{E4}\right)\right)\right)\right) \\ F_R^{out} = RCAB\left(ESA\left(Conv\_3\left(Cat\left(F_R^{D1}, F_R^{D2}, F_R^{D3}, F_R^{E4}\right)\right)\right)\right) \end{cases}, \tag{2}$$

where $F_L^{D1,2,3,4}$and $F_R^{D1,2,3,4}$ represent distilled features, $F_L^{E1,2,3,4}$ and $F_R^{E1,2,3,4}$ represent enhanced features. "Cat" denotes the concatenation operation, which integrates diverse features from the distilled and enhanced images. ESA designed to boost spatial features within the image. RCAB, as shown in Fig. 2e, is based on the channel attention (CA) [31] mechanism. It includes two channel adjustment convolutional operations before CA, where the first convolution is used for channel compression and the second convolution, after the GELU activation function, is used for channel expansion. A residual connection is introduced in the channel attention convolution block before CA to alleviate the impact of insufficient channel representation before entering CA. Introducing both spatial and channel attention mechanisms can enhance the representation capability of the feature distillation and enhancement module while maintaining the model's efficiency [35].

3.4 *Residual Epipolar Line Window Attention (REWA)*

To utilize complementary information in the images, we designed the REWA operation, which aggregates fusion features at different levels by connecting several EWA modules in a residual manner.

As shown in Fig. 2f, REWA connects multiple EWA modules using a residual approach to aggregate fusion features. While the PAM efficiently promotes the alignment of left and right views using epipolar geometry constraints in stereo vision, it is observed that corresponding pixels may appear at different positions along the epipolar line, as depicted in Fig. 3. Moreover, in regions with smooth pixels like the sky, where there are no clear reference points, the accuracy of the alignment operation can be affected. Fig. 4 illustrates a comparison between our EWA, self-attention [51], and PAM. Self-attention is a method for calculating the correlation between pixels in an image, which is used to learn the dependencies between pixels and address long-range dependencies and translational invariance issues in image tasks. PAM is based on self-attention and is used to learn the similarity relationships between stereo images, resulting in a disparity map that promotes better alignment between the left and right images. Inspired by self-attention and PAM, our EWA can concentrate on pixels within windows along the epipolar line, improving the accuracy of left and right view alignment. For areas with small pixel value fluctuations, EWA can effectively use neighboring pixels within the window as references, enhancing the efficiency of left and right view alignment. EWA, as shown in Fig. 5, first divides the input feature map into $M_1 \times W$ windows, where M_1 represents the window's height, and following the principles of Swin Transformer window division, we set $M_1 = 6$. W represents the original width of the feature map. The left and right view windows corresponding to the corresponding areas are then fed into the cross-view attention model (CAM), which is illustrated in Fig. 5a. CAM is based on self-attention and PAM, and it computes the similarity between the left and right stereo views using query and key sources that are not the same, fusing complementary information. Given input window features F_L^{Window} and F_R^{Window} for the left and right views, the CAM operation is as follows:

$$F_L^{CAM}, F_R^{CAM} = CAM\left(F_L^{Window}, F_R^{Window}\right), \tag{3}$$

Following [6,52], we propose CAM, which enables the network to learn the correspondence between stereo images. Since we have known from [6] that there is a mapping relationship between pixels, and via feature fusion in [52], we propose to fuse the features of the left and right images as:

$$F_{L \text{ or } R}^{CAM} = F_{L \text{ or } R}^{Window} + \lambda F_{R \text{ or } L}^{Window}, \tag{4}$$

Taking the left view fused feature as an example, where λrefers to the spatial importance weight for the feature maps of F_L^{Window} and F_R^{Window}, which is adaptively learned by the network. Inspired by [52], we force $\lambda \in [0, 1]$, which is defined by using self-attention with $Q \in \mathbb{R}^{H \times W \times C_1}$ and $K \in \mathbb{R}^{H \times W \times C_1}$ as control parameters, respectively. We use layer normalized and a channel attention convolution layer to get the weight maps Q and K from F_L^{Window} and F_R^{Window}, respectively, and they can thus be learned through back-propagation of the network.

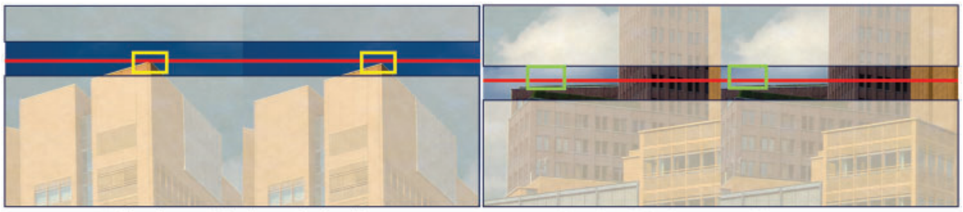
(a) Pixels outside the epipolar line

(b) Pixels in the smoothing area

Figure 3: Relationship of pixels in epipolar line. (a) represents the case where pixels appear outside the epipolar line. (b) represents the case where features on the epipolar line are in the background region

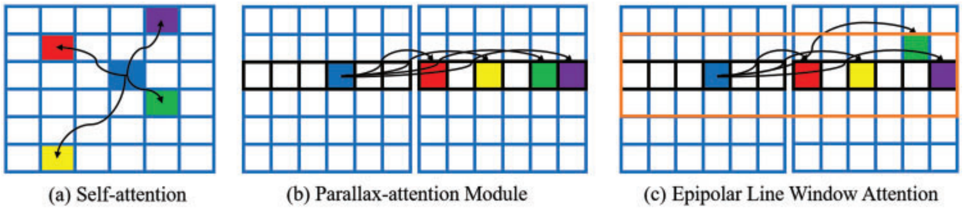

(a) Self-attention

(b) Parallax-attention Module

(c) Epipolar Line Window Attention

Figure 4: Schematic of the epipolar line window. These arrows represent the similarity relationships between the blue pixels and other color pixels. Orange box represents epipolar line window

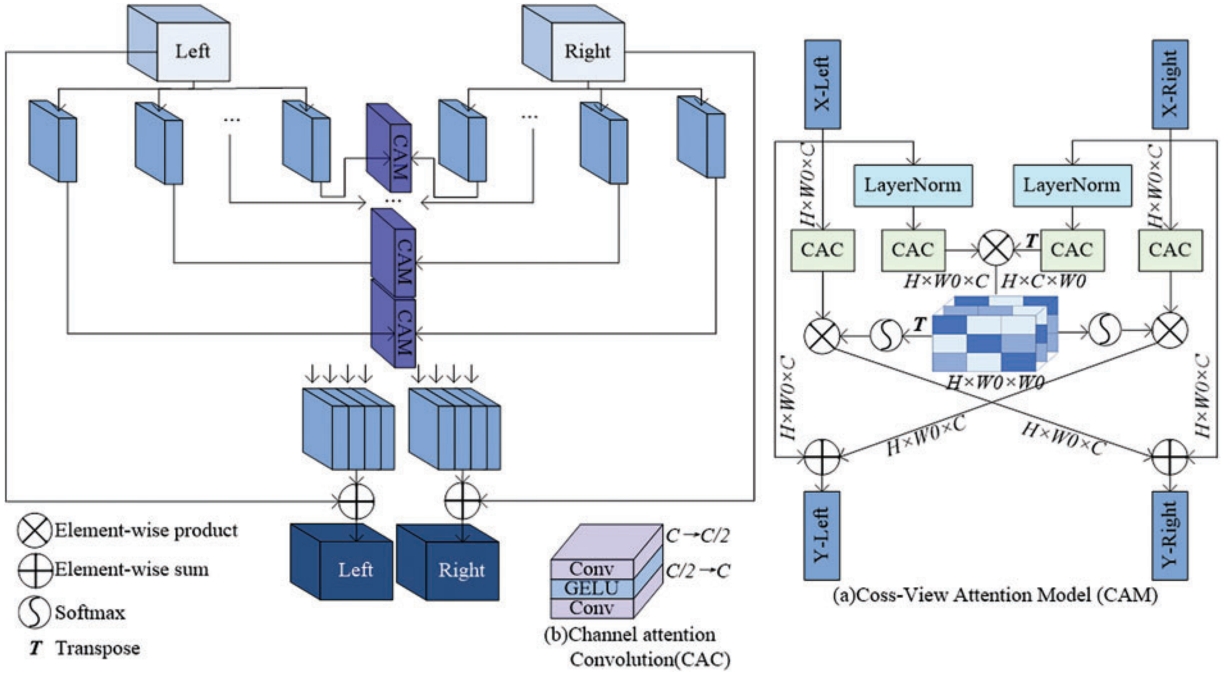

(b)Channel attention Convolution(CAC)

(a)Coss-View Attention Model (CAM)

Figure 5: Epipolar line window attention. The blue rectangular box represents the partitioned window along the epipolar line, and the overlaid blue rectangular box represents the features fused by CAM along the width dimension of the image

In detail, as shown in Fig. 5a, in CAM we first calculate the dot product of all keys of the query and apply a softmax function to derive the weights of the values:

$$\text{Attention}\,(Q, K, V) = \text{SoftMax}\left(QK^T/\sqrt{d}\right) V, \tag{5}$$

where Q is query matrix from the source view feature (e.g., F_L^{Window}), and K and $V \in \mathbb{R}^{H\times W\times C_1}$ are key and value matrices, respectively, both projected from the source view feature (e.g., F_R^{Window}). Taking the left view as an example, F_L^{Window} is fed to layer normalized and a channel attention convolution (CAC) to produce Q, Meanwhile, F_R^{Window} is fed to another layer normalized and a CAC to produce K, which is then reshaped to $K^{-1} \in \mathbb{R}^{H\times d\times W}$. The softmax layer is then applied after applying matrix multiplication between Q and K, resulting in a Similarity weight value λ. Next, F_R^{Window} is passed to a CAC to generate V, which is matrix multiplied with λ to obtain the complementary information of F_R^{Window} to F_L^{Window}. Finally a residual structure is introduced to obtain the fused image. As shown in Fig. 5b, by applying CAC before the cross-view point convolution, the weights between the depth feature channels can be adaptively adjusted, which helps to effectively utilize complementary information in the image. To integrate the disparity maps from each epipolar line window, within EWA, we concatenate the results obtained from CAM to obtain a complete set of left and right complementary views.

3.5 Loss

For better constraining the reconstruction relationship between high-resolution and low-resolution images, we optimize the parameters of EWASSR by mean square error (MSE) loss:

$$Loss = \|I_S - I_H\|, \tag{6}$$

where I_S is the output from EWASSR, and I_H represents the corresponding groundtruth of stereo images.

4 Experiments

4.1 Implementation Details

We followed [42,52] and used 800 stereo images from the training set of Flickr1024 and 60 stereo images from Middlebury as the training data. For test, we used 5 images from the Middlebury dataset, 20 images from the KITTI 2012 dataset and 20 images from the KITTI 2015 dataset as benchmark datasets. The test set images were obtained by bicubic downsampling. For validation, we used an additional 20 images from the KITTI 2012 dataset. Middlebury is used to evaluate disparities. KITTI includes vehicle and pedestrian images with various degrees of occlusion and truncation. Flickr1024 contains high-quality stereo images of multiple scene categories for super-resolution reconstruction. These real datasets provide a range of disparities and occlusions, better reflecting the challenges and issues encountered in practical super-resolution reconstruction scenarios for stereo images.

We cropped the LR and HR images to 30×90 patches with a step size of 20 [42,52]. These patches are randomly flipped to achieve data enhancement. Our EWASSR was implemented in Pytorch on a PC with an Nvidia RTX 4090 GPU. All models were optimized using the Adam method with $\beta1 = 0.9$, $\beta2 = 0.999$ and a batch size of 8. The initial learning rate was set to 2×10^{-4} and reduced to half after every 30 epochs. The training was stopped after 80 epochs since more epochs do not provide further consistent improvement. In our network model, the RSTFB number, EWA number, STFL number, window size, channel number and attention head number are generally set to 8, 8, 6, 6, 96 and 4, respectively. We use peak signal-to-noise ratio (PSNR) and structural similarity index measurement (SSIM) as the SR result evaluation metrics [7], because they can directly reflect the quality of the image by comparing the degree of difference between the original image and the processed image. We use the number of parameters and FLOPs as performance metrics for judging the model. The number of parameters reflects the complexity of the model, while FLOPs reflect the computational efficiency and speed of the model. The combination of the two can evaluate the performance of the model more comprehensively.

4.2 Ablation Study

To demonstrate the choice of our network, we perform 4× scaling experiments on the KITTI2015 test set, where the experiments are illustrated in two parts: the feature extraction module and the feature fusion module.

4.2.1 Swin Transformer FDEB Layer

To demonstrate the effectiveness of our EWASSR with (S)W-MSA and FDEB, we introduced three variants. As shown in Table 1, Nr.1 represents the experimental results for our network, with the

"Value" column showing the PSNR results compared to our EWASR as the baseline. First, to validate the effectiveness of introducing FDEB in STL, we removed FDEB in the baseline network, using only the Transformer-based structure for feature extraction. The results for Nr.2 confirm that removing FDEB resulted in a decrease in PSNR by 0.59 dB. This is because the feature extractor based on the Transformer does not pay enough attention to local details, resulting in incomplete high-frequency feature restoration. Then, following the reference [35], we replaced FDEB in the network with the channel attention block (CAB). However, the experimental results decreased to 26.54 dB. Finally, we replaced FDEB with NAFblock, and the results showed a PSNR reduction of 0.48 dB. The results for these three variants demonstrate the effectiveness of our chosen feature extraction module, achieving performance improvement while adding only a negligible number of parameters.

Table 1: Results achieved on the KITTI2015 dataset by EWASSR with different settings in feature extraction for 4× SR

Nr	Model	PSNR (dB)	Value (dB)	SSIM	#Params.	GFLOPs input size (30 × 90)
1	EWASSR	26.87	refer	0.8215	1.35M	34.29
2	EWASSR without FDEB	26.28	−0.59	0.8004	0.81M	22.76
3	EWASSR with CBM [35]	26.54	−0.33	0.8037	1.22M	31.14
4	EWASSR with NAFblock [6]	26.39	−0.48	0.8025	1.28M	31.67

4.2.2 Residual Epipolar Line Window Attention

To effectively utilize complementary information in stereo images, we proposed a cross-view fusion attention network along the epipolar line partition. We designed four variants for experimentation. As shown in Table 2, first, we removed EWA from EWASSR, using a simple element-wise summation operation, resulting in a significant decrease in the PSNR value (decreased by 0.9 dB). The re-fusion of features from EWA outputs at different network depths allows for the integration of complementary information. We attempted to remove REWA, and the experimental results for Nr.3 showed that without secondary fusion, the network's PSNR performance decreased to 26.73 dB. To demonstrate the effectiveness of EWA in partitioned window operations, we compared two disparity attention modules. First, we replaced our EWA with SCAM, and we found that the PSNR value of the network decreased by 0.34 dB. Next, we replaced EWA with ibPAM, and from Nr.5, despite an increase in network parameters, the PSNR did not improve and instead decreased by 0.54 dB. These series of experimental results confirm that partitioned window operations with geometric constraints improve the accuracy of complementary information in the fusion process.

Additionally, as shown in Fig. 6, we conducted a visual analysis of the intermediate features of EWA and SCAM. The figure shows the results of the "Middlebury-Motorcycle" for 4×. Blue to red represents the increasing attention of the network. We selected the more complex area of the engine part for comparison, and the red area of EWA is more abundant than SCAM. This is because EWA focuses on the features along the epipolar line window, making the feature area of interest more comprehensive. Experiments have shown that EWA exhibits higher attention in complex texture areas, which helps to recover high-frequency features of the image.

Table 2: Results achieved on the KITTI2015 dataset by EWASSR with different settings in feature fusion for 4× SR

Nr	Models	PSNR (dB)	Value (dB)	SSIM	#Params.	GFLOPs input size (30 × 90)
1	EWASSR	26.87	refer	0.8215	1.35 M	34.29
2	EWASSR without EWA	25.97	−0.90	0.7914	1.31 M	33.58
3	EWASSR without REWA	26.73	−0.14	0.8208	1.35 M	34.29
4	EWASSR with SCAM [6]	26.53	−0.34	0.8121	1.35 M	34.29
5	EWASSR with ibPAM [48]	26.33	−0.54	0.8088	1.36 M	35.30

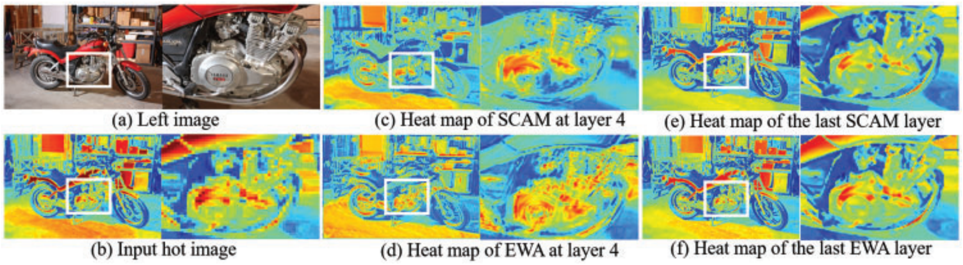
(a) Left image
(c) Heat map of SCAM at layer 4
(e) Heat map of the last SCAM layer
(b) Input hot image
(d) Heat map of EWA at layer 4
(f) Heat map of the last EWA layer

Figure 6: Feature images during feature fusion

4.3 *Comparison to State-of-the-Arts*

In this section, we compare EWASSR with various state-of-the-art methods, such as VDSR [53], RDN [54], RCAN [30], StereoSR [2], PASSRnet [42], iPASSR [48], SSRDE-FNet [9], and NAFSSR [6]. It is important to mention that all these methods are trained on identical datasets as ours.

4.3.1 *Quantitative Results*

As shown in Table 3, we compared our EWASSR with classical and advanced networks in Stereo SR tasks. The table indicates that EWASSR outperforms advanced networks in stereo super-resolution tasks. Analyzing the results from the four datasets, our network exhibits superior SR performance in three of them, except for the KITTI2012 dataset, where the improvement is less pronounced. Our network demonstrates significant performance improvements on the Middlebury and Flickr1024 test sets. Specifically, in the 2× experiments, compared to the representative network NAFFSSR-S, our network achieved an increase of 0.37 and 0.34 dB in PSNR, as well as SSIM improvements of 0.0025 and 0.0054 on the Middlebury and Flickr1024 test sets, respectively. In the 4× experiments, our network improved PSNR by 0.16 and 0.14 dB on these two datasets. It is worth noting that we chose NAFFSSR-S as a comparison network because its parameter count is in the same range as our network. In the results using only the left image as input, we observed that on the KITTI2012 test set, our network slightly lags NAFFSSR-S. This is due to the input being the same for the left and right images, meaning our EWA did not effectively utilize complementary information, resulting in similar performance to the non-partitioned disparity attention results.

Table 3: Quantitative results achieved by different methods in four stereo datasets. PSNR/SSIM values achieved on both the left images (i.e., Left) and a pair of stereo images (i.e., (Left + Right)/2) are reported. Our network is in bold font and the best result is red

Method	Scale	#Params.	Left PSNR (dB)/SSIM			(Left + Right)/2 PSNR (dB)/SSIM			
			Middlebury	KITTI2012	KITTI2015	Middlebury	KITTI2012	KITTI2015	Flickr1024
VDSR [53]	×2	0.66 M	32.66/0.9101	30.17/0.9062	28.99/0.9038	32.77/0.9102	30.30/0.9089	29.78/0.9150	25.60/0.8534
RDN [54]	×2	22.0 M	34.85/0.9488	30.81/0.9197	29.91/0.9224	34.94/0.9491	30.94/0.9227	30.70/0.9330	28.64/0.9084
RCAN [30]	×2	15.3 M	34.80/0.9482	30.88/0.9202	29.97/0.9231	34.90/0.9486	31.02/0.9232	30.77/0.9336	28.63/0.9082
StereoSR [2]	×2	1.08 M	33.15/0.9343	29.42/0.9040	28.53/0.9038	33.23/0.9348	29.51/0.9073	29.33/0.9168	25.96/0.8599
PASSRnet [42]	×2	1.37 M	34.13/0.9421	30.68/0.9159	29.81/0.9191	34.23/0.9422	30.81/0.9190	30.60/0.9300	28.38/0.9038
iPASSR [48]	×2	1.37 M	34.41/0.9454	30.97/0.9210	30.01/0.9234	34.51/0.9454	31.11/0.9240	30.81/0.9340	28.60/0.9097
SSRDE-FNet [9]	×2	2.10 M	35.02/0.9508	31.08/0.9224	30.10/0.9245	35.09/0.9511	31.23/0.9254	30.90/0.9352	28.85/0.9132
NAFSSR-S [6]	×2	1.54 M	35.23/0.9515	31.23/0.9236	30.28/0.9266	35.30/0.9514	31.38/0.9266	31.08/0.9367	29.19/0.9160
EWASSR (Ours)	**×2**	**1.24 M**	**35.36/0.9528**	**31.20/0.9232**	**30.33/0.9268**	**35.67/0.9539**	**31.38/0.9271**	**31.17/0.9371**	**29.53/0.9214**
VDSR [53]	×4	0.66 M	27.60/0.7933	25.54/0.7662	24.68/0.7456	27.69/0.7941	25.60/0.7722	25.32/0.7703	22.46/0.6718
RDN [54]	×4	22.0 M	29.18/0.8387	26.23/0.7952	25.37/0.7813	29.27/0.8404	26.32/0.8014	26.04/0.8043	23.47/0.7295
RCAN [30]	×4	15.4 M	29.20/0.8381	26.36/0.7968	25.53/0.7836	29.30/0.8397	26.44/0.8029	26.22/0.8068	23.48/0.7286
StereoSR [2]	×4	1.42 M	27.70/0.8036	24.49/0.7502	23.67/0.7273	27.64/0.8022	24.53/0.7555	24.21/0.7511	21.70/0.6460
PASSRnet [42]	×4	1.42 M	28.61/0.8232	26.26/0.7919	25.41/0.7772	28.72/0.8236	26.34/0.7981	26.08/0.8002	23.31/0.7195
SSRes+SAM [47]	×4	1.73 M	28.76/0.8287	26.35/0.7957	25.55/0.7825	28.83/0.8290	26.44/0.8018	26.22/0.8054	23.27/0.7233
iPASSR [48]	×4	1.42 M	29.07/0.8363	26.47/0.7993	25.61/0.7850	29.16/0.8367	26.56/0.8053	26.32/0.8084	23.44/0.7287
SSRDE-FNet [9]	×4	2.24 M	29.29/0.8407	26.61/0.8028	25.74/0.7884	29.38/0.8411	26.70/0.8082	26.43/0.8118	23.59/0.7352
NAFSSR-S [6]	×4	1.56 M	29.62/0.8482	26.84/0.8086	26.03/0.7978	29.72/0.8490	26.93/0.8145	26.76/0.8203	23.88/0.7468
EWASSR (Ours)	**×4**	**1.35 M**	**29.68/0.8483**	**26.81/0.8077**	**26.09/0.7981**	**29.88/0.8516**	**26.94/0.8140**	**26.87/0.8215**	**24.02/0.7474**

As shown in Table 4, to analyze the model complexity, we selected the classical Stereo SR networks for comparison. The results in the table show that our network has the smallest number of parameters, but not the lowest computational effort, which is related to the depth of our network. Overall, we analyze that we have improved the SR performance by increasing only a small amount of computation while maintaining a better number of parameters.

Table 4: Comparison of model complexity of different methods in "Middlebury-sword2"

Method	Scale	#Params.	GFLOPs	PSNR (dB)	SSIM
PASSRnet [42]	×4	1.42 M	55.34	31.99	0.9035
iPASSR [48]	×4	1.42 M	64.31	33.09	0.9165
SSRDE-FNet [9]	×4	2.24 M	580.03	33.19	0.9187
NAFSSR-S [6]	×4	1.56 M	55.44	33.92	0.9237
EWASSR (Ours)	×4	1.35 M	69.02	34.00	0.9240

4.3.2 Qualitative Results

We randomly selected a pair of stereo images from each of the four datasets as test data and presented the comparison results for 4× SR of the left and right images. In the results of Fig. 7, our EWASSR brings out the stereo contours of the folders and swords more effectively. In Fig. 8, none of the networks exhibit exceptional visual performance, mainly due to the presence of considerable noise in this test image. Upon close examination of the visual results, our network still outperforms the others. In Fig. 9, our EWASSR presents signs and zebra crossings that are closer to the ground truth (GT) images. As for building recovery, as shown in Fig. 10, EWASSR achieves the best visual performance.

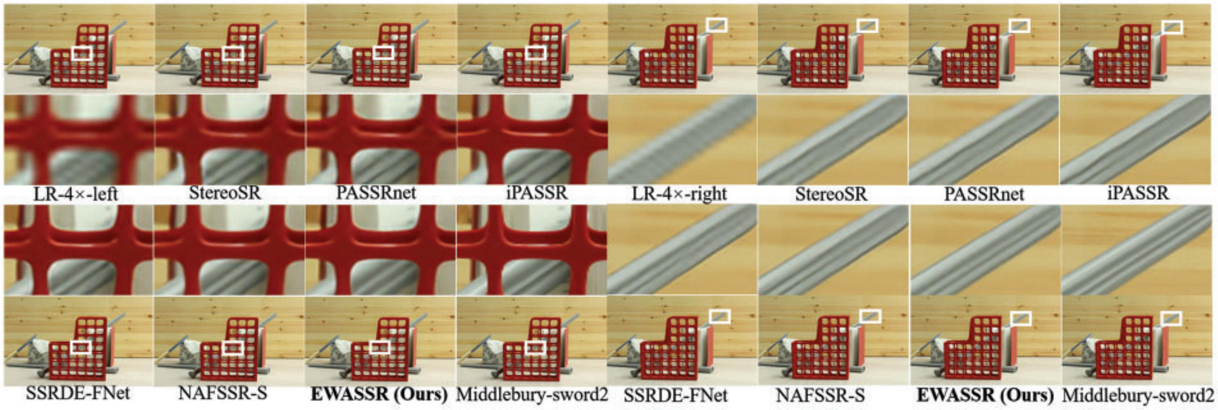

Figure 7: "Middlebury-sword2" comparison of visualization results for 4× SR

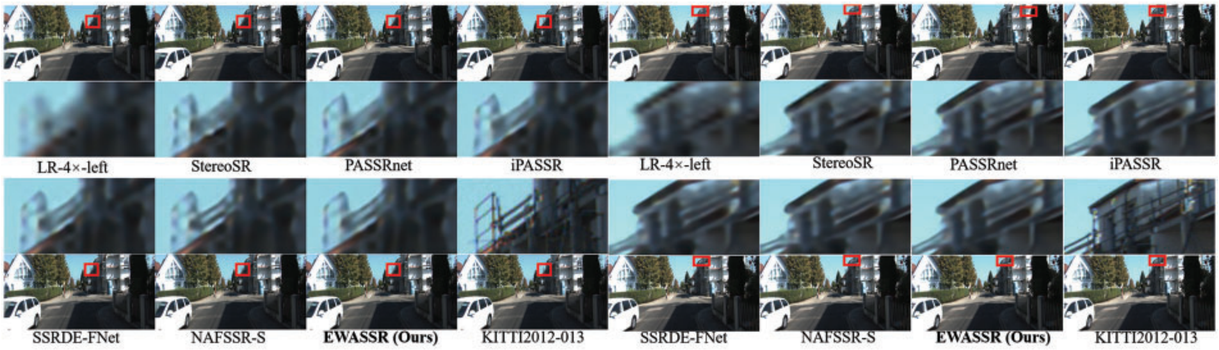

Figure 8: "KITTI2012-013" comparison of visualization results for 4× SR

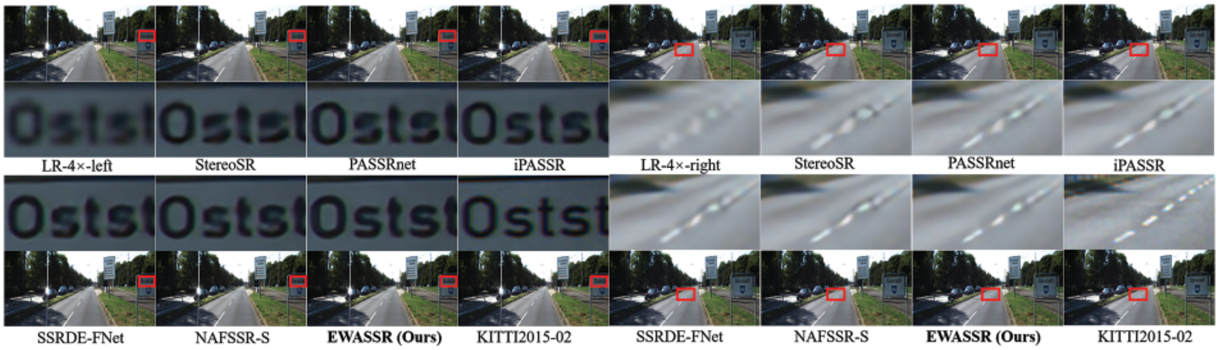

Figure 9: "KITTI2015-02" comparison of visualization results for 4× SR

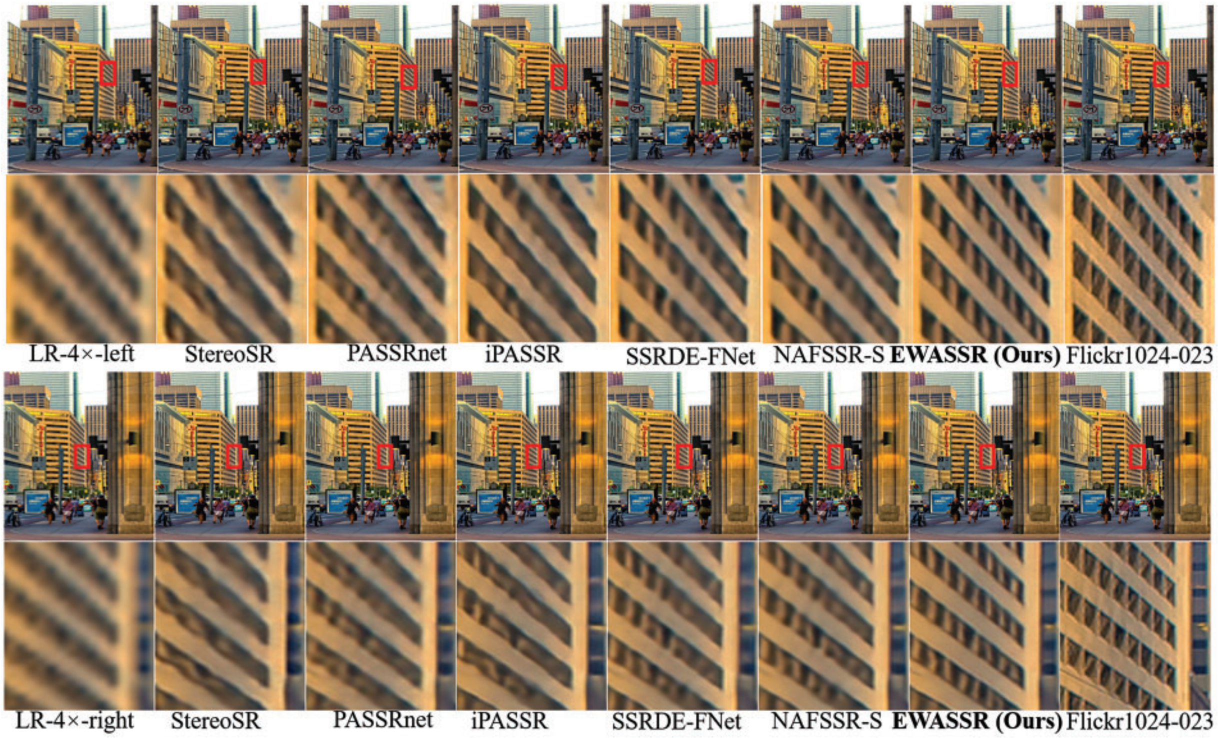

Figure 10: “Flickr1024-023” comparison of visualization results for 4× SR

5 Conclusion

In this paper, we propose an attention network, named EWASSR, which partitions windows along the epipolar line to address the challenges of high-frequency feature reconstruction and complementary information fusion in Stereo SR tasks. The conclusions are summarized as follows:

(1) Designed the RSTFB hybrid feature extraction module, significantly enhancing the network’s ability to capture high-frequency features by establishing long-range dependencies between images. The effectiveness of our network in image SR performance has been demonstrated, with a 0.59 dB increase in PSNR after introducing the FDEB module, further confirming its outstanding performance.

(2) The EWA module has become a critical component of the network, enabling it to learn the similarity between points in one view and pixels within epipolar line window in another view. The key role of this module lies in effectively integrating complementary information from stereo images, enhancing the model’s understanding of image structure.

(3) The REWA module has made a significant contribution to the effective fusion of complementary disparity attention maps. It achieves this by performing a secondary fusion of the disparity maps obtained through EWA, integrating features from different levels and scales.

(4) In quantitative evaluations, when provided with left and right views as input, EWASSR outperforms previous methods across four publicly available datasets, showcasing its exceptional performance in SR and confirming its continuous improvement over existing methods.

(5) Qualitative evaluations highlight the efficiency of EWASSR in generating visual results similar to GT images. This capability underscores the practical value of the model in enhancing image quality.

The research demonstrates that our EWASSR achieves outstanding SR performance while maintaining a relatively low parameter count. However, during the experiments, we identified areas for improvement in our model. Specifically, insufficient attention to view-specific information led to suboptimal performance under single inputs. Additionally, the method may face limitations in scenarios with motion blur, such as in the KITTI dataset. Therefore, designing an efficient and high-performance Stereo SR network is a major challenge in the current field. Future research will focus on image super-resolution in complex environments, combining attention to image-specific information and noise reduction to further optimize the method for broader applications.

Acknowledgement: The authors would like to thank the editors and reviewers for their valuable work.

Funding Statement: This work was supported by Sichuan Science and Technology Program (2023YFG0262).

Author Contributions: The authors confirm contribution to the paper as follows: Study conception and design: Xue Li, Hongying Zhang; data collection: Zixun Ye, Xiaoru Huang; analysis and interpretation of results: Xue Li, Hongying Zhang; draft manuscript preparation: Xue Li, Zixun Ye, Xiaoru Huang. All authors reviewed the results and approved the final version of the manuscript.

Availability of Data and Materials: The data that support the findings of this study are available from the first author, Xue Li, upon reasonable request.

Conflicts of Interest: The authors declare that they have no conflicts of interest to report regarding the present study.

References

[1] V. A. Bhavsar and A. N. Rajagopalan, “Resolution enhancement in multi-image stereo,” *IEEE Trans. Pattern Anal. Mac. Intell.*, vol. 32, no. 9, pp. 1721–1728, 2010. doi: 10.1109/TPAMI.2010.90.

[2] D. S. Jeon, S. H. Baek, I. Choi, and M. H. Kim, “Enhancing the spatial resolution of stereo images using a parallax prior,” in *Proc. Comput. Vis. Pattern Recognit. (CVPR)*, Salt Lake City, UT, USA, 2018, pp. 1721–1730.

[3] J. Zou, Z. Li, Z. Guo, and D. Hong, “Super-resolution reconstruction of images based on microarray camera,” *Comput. Mater. Continua*, vol. 60, no. 1, pp. 163–177, 2019. doi: 10.32604/cmc.2019.05795.

[4] H. Sheng, S. Z. Wang, D. Yang, R. X. Cong, and Z. L. Cui, “Cross-view recurrence-based self-supervised super-resolution of light field,” *IEEE Trans. Circ. Syst. Vid. Tech.*, vol. 33, no. 12, pp. 7252–7266, 2023. doi: 10.1109/TCSVT.2023.3278462.

[5] Z. Hui, J. Li, X. B. Gao, and X. M. Wang, “Progressive perception-oriented network for single image super-resolution,” *Inform. Sci.*, vol. 546, pp. 769–786, 2021. doi: 10.1016/j.ins.2020.08.114.

[6] X. J. Chu, L. G. Chen, and W. Q. Yu, “NAFSSR: Stereo image super-resolution using NAFNet,” in *Proc. Comput. Vis. Pattern Recognit. (CVPR)*, New Orleans, LA, USA, 2022, pp. 1239–1248.

[7] X. Y. Zhu, K. H. Guo, H. Fang, L. Chen, S. Ren and B. Hu, “Cross view capture for stereo image super-resolution,” *IEEE Trans. Multimed.*, vol. 546, pp. 3074–3086, 2021. doi: 10.1109/TMM.2021.3092571.

[8] J. X. Lin, L. Y. Yin, and Y. J. Wang, “Steformer: Efficient stereo image super-resolution with transformer,” *IEEE Trans. Multimed.*, vol. 25, pp. 8396–8407, 2023. doi: 10.1109/TMM.2023.3236845.

[9] Q. Y. Dai, J. C. Li, Q. S. Yi, F. M. Fang, and G. X. Zhang, “Feedback network for mutually boosted stereo image super-resolution and disparity estimation,” in *Proc. ACM Int. Conf. Multimed. (ACM MM)*, Bejing, China, 2021, pp. 1985–1993.

[10] W. Y. Ying, T. Y. Dong, and S. T. Chen, “Accurate stereo image super-resolution using spatial-attention-enhance residual network,” *Multimed. Tools Appl.*, vol. 10, no. 11, pp. 12117–12133, 2023. doi: 10.1007/s11042-022-13815-x.

[11] K. Jiang, Z. Y. Wang, P. Yi, J. J. Jiang, J. Xiao and Y. Yao, “Deep distillation recursive network for remote sensing imagery super-resolution,” *Remote Sens.*, vol. 10, no. 11, pp. 1700–1722, 2018.

[12] Z. Hui, X. B. Gao, and X. M. Wang, “Lightweight image super-resolution with feature enhancement residual network,” *Neurocomputing*, vol. 404, pp. 50–60, 2020. doi: 10.1016/j.neucom.2020.05.008.

[13] W. M. Yang, W. Wang, X. C. Zhang, S. F. Su, and Q. M. Liao, “Lightweight feature fusion network for single image super-resolution,” *IEEE Signal Proc. Let.*, vol. 26, no. 4, pp. 538–542, 2019. doi: 10.1109/LSP.2018.2890770.

[14] X. Tan, C. M. Sun, X. Sirault, R. Furbank, and T. D. Pham, “Stereo matching using cost volume watershed and region merging,” *Signal Proc.: Image Commun.*, vol. 29, no. 10, pp. 1232–1244, 2014. doi: 10.1016/j.image.2014.06.002.

[15] Z. F. Liang *et al.*, “Stereo matching using multi-level cost volume and multi-scale feature constancy,” *IEEE Trans. Pattern Anal. Mach. Intell.*, vol. 43, no. 1, pp. 300–315, 2019. doi: 10.1109/TPAMI.2019.2928550.

[16] J. Wan, H. Yin, and Z. H. Liu, “Multi-stage edge-guided stereo feature interaction network for stereoscopic image super-resolution,” *IEEE Trans. Broadcast*, vol. 69, no. 2, pp. 357–368, 2023. doi: 10.1109/TBC.2023.3264880.

[17] Z. H. Wan, C. Jia, and C. Steven, “Deep learning for image super-resolution: A survey,” *IEEE Trans. Pattern Anal. Mach. Intell.*, vol. 43, no. 10, pp. 3365–3387, 2020. doi: 10.1109/TPAMI.2020.2982166.

[18] C. Dong, C. C. Loy, K. He, and X. Tang, “Image super-resolution using deep convolutional networks,” *IEEE Trans. Pattern Anal. Mach. Intell.*, vol. 38, no. 2, pp. 295–307, 2015. doi: 10.1109/015.2439281.

[19] Z. D. Zhang, X. R. Wang, and C. K. Jung, “DCSR: Dilated convolutions for single image super-resolution,” *IEEE Trans. Image Process.*, vol. 28, no. 4, pp. 1625–1635, 2018. doi: 10.1109/TIP.2018.2877483.

[20] Y. F. Wang, L. J. Wang, H. Y. Wang, and P. H. Li, “End-to-end image super-resolution via deep and shallow convolutional networks,” *IEEE Access*, vol. 7, pp. 31959–31970, 2019. doi: 10.1109/ACCESS.2019.2903582.

[21] X. Che and C. W. Sun, “Multiscale recursive feedback network for image super-resolution,” *IEEE Access*, vol. 10, pp. 6393–6406, 2022. doi: 10.1109/ACCESS.2022.3142510.

[22] C. Yang and G. M. Lu, “Deeply recursive low-and high-frequency fusing networks for single image super-resolution,” *Sens.*, vol. 20, no. 24, pp. 7268–77285, 2020. doi: 10.3390/s20247268.

[23] W. H. Yang *et al.*, “Deep edge guided recurrent residual learning for image super-resolution,” *IEEE Trans. Image Process.*, vol. 26, no. 12, pp. 5895–5907, 2017. doi: 10.1109/TIP.2017.2750403.

[24] J. W. Xin, J. Li, X. R. Jiang, and N. N. Wang, “Wavelet-based dual recursive network for image super-resolution,” *IEEE Trans. Neur. Netw. Learn. Syst.*, vol. 33, no. 2, pp. 707–720, 2020. doi: 10.1109/TNNLS.2020.3028688.

[25] S. Anwar and N. Barne, “Densely residual laplacian super-resolution,” *IEEE Trans. Pattern Anal. Mach. Intell.*, vol. 44, no. 3, pp. 1192–1204, 2020. doi: 10.1109/TPAMI.2020.3021088.

[26] L. Sun, Z. B. Liu, X. Y. Sun, L. C. Liu, R. S. Lan and X. N. Luo, “Lightweight image super-resolution via weighted multi-scale residual network,” *IEEE/CAA J. Autom. Sin.*, vol. 8, no. 7, pp. 1271–1280, 2021. doi: 10.1109/JAS.2021.1004009.

[27] H. Li and F. L. Cao, “Lightweight image super-resolution via weighted multi-scale residual network,” *Neural Netw.*, vol. 13, pp. 84–95, 2020. doi: 10.1109/JAS.2021.1004009.

[28] J. C. Li, F. M. Fang, J. Q. Li, K. F. Mei, and G. X. Zhang, “MDCN: Multi-scale dense cross network for image super-resolution,” *IEEE Trans. Circ. Syst. Vid. Technol.*, vol. 31, no. 7, pp. 2547–2561, 2020. doi: 10.1109/TCSVT.2020.3027732.

[29] K. Yang *et al.*, “Residual feature attentional fusion network for lightweight chest CT image super-resolution,” *Comput. Mater. Continua*, vol. 75, no. 3, pp. 5159–5176, 2023. doi: 10.32604/cmc.2023.036401.

[30] Y. Zhang, K. Li, K. Li, L. Wang, B. Zhong and Y. Fu, "Image super-resolution using very deep residual channel attention networks," in *Proc. Eur. Conf. Comput. Vis. (ECCV)*, Munich, Germany, 2018, pp. 286–301.

[31] E. M. Lu and X. X. Hu, "Image super-resolution via channel attention and spatial attention," *Appl. Intell.*, vol. 52, no. 2, pp. 2260–2268, 2022. doi: 10.1007/s10489-021-02464-6.

[32] S. Khan, M. Naseer, M. Hayat, S. W. Zamir, F. S. Khan and M. Shah, "Transformers in vision: A survey," *ACM Comput. Surv.*, vol. 54, no. 10s, pp. 1–41, 2022. doi: 10.1145/3505244.

[33] Q. P. Jiang *et al.*, "Single image super-resolution quality assessment: A real-world dataset, subjective studies and an objective metric," *IEEE Trans. Image Proc., 2023*, vol. 31, pp. 2279–2294, 2022. doi: 10.1109/TIP.2022.3154588.

[34] C. Saharia, J. Ho, W. Chan, T. Salimans, D. J. Fleet and M. Norouzi, "Image super-resolution via iterative refinement," *IEEE Trans. Pattern Anal. Mach. Intell.*, vol. 45, no. 4, pp. 4713–4726, 2023. doi: 10.1109/TPAMI.2022.3204461.

[35] X. Y. Chen, X. T. Wang, and J. T. Zhou, "Activating more pixels in image super-resolution transformer," in *Proc. Comput. Vis. Pattern Recognit. (CVPR)*, Vancouver, Canada, 2023, pp. 22367–22377.

[36] A. M. Ali, B. Benjdira, A. Koubaa, W. El-Shafai, Z. Khan and B. Khan, "Vision transformers in image restoration: A survey," *Sens.*, vol. 23, no. 5, pp. 2385–2407, 2023. doi: 10.3390/s23052385.

[37] A. Mehri, P. Behjati, D. Carpio, S. Bai, and A. D. Sappa, "SRFormer: Efficient yet powerful transformer network for single image super resolution," *IEEE Access*, vol. 11, pp. 121457–121469, 2023. doi: 10.1109/ACCESS.2023.3328229.

[38] S. Park and Y. S. Choi, "Image super-resolution using dilated window transformer," *IEEE Access*, vol. 11, pp. 60028–60039, 2023. doi: 10.1109/ACCESS.2023.3284539.

[39] J. Liu, J. Tang, and G. S. Wu, "Residual feature distillation network for lightweight image super-resolution," in *Proc. Eur. Conf. Comput. Vis. (ECCV)*, Glasgow, UK, 2020, pp. 41–55.

[40] X. Qiao, C. Y. Ge, and P. C. Deng, "Depth restoration in under-display time-of-flight imaging," *IEEE Trans. Pattern Anal. Mach. Intell.*, vol. 45, no. 5, pp. 5668–5683, 2022. doi: 10.1109/TPAMI.2022.3209905.

[41] T. Y. Zhang, Y. Gu, and X. L. Huang, "Disparity-constrained stereo endoscopic image super-resolution," *Int. J. Comput. Asst. Radiol. Surg.*, vol. 17, no. 5, pp. 867–875, 2022. doi: 10.1007/s11548-022-02611-5.

[42] L. G. Wang *et al.*, "Learning parallax attention for stereo image super-resolution," in *Proc. Comput. Vis. Pattern Recognit. (CVPR)*, Long Beach, CA, USA, 2019, pp. 12250–12259.

[43] L. G. Wang *et al.*, "Parallax attention for unsupervised stereo correspondence learning," *IEEE Trans. Pattern Anal. Mach. Intell.*, vol. 44, no. 4, pp. 2108–2125, 2020. doi: 10.1109/TPAMI.2020.3026899.

[44] W. Song, S. Choi, S. Jeong, and K. Sohn, "Stereoscopic image super-resolution with stereo consistent feature," in *Proc. AAAI Conf. Artif. Intell.*, vol. 34, no. 7, pp. 12031–12038, 2020. doi: 10.1609/aaai.v34i07.6880.

[45] J. J. Lei *et al.*, "Deep stereoscopic image super-resolution via interaction module," *IEEE Trans. Circ. Syst. Video Technol.*, vol. 31, no. 8, pp. 3051–3061, 2021. doi: 10.1109/TCSVT.2020.3037068.

[46] C. Q. Chen, C. M. Qing, X. M. Xu, and P. Dickinson, "Cross parallax attention network for stereo image super-resolution," *IEEE Trans. Multimed.*, vol. 2, pp. 202–216, 2021. doi: 10.1109/TMM.2021.3050092.

[47] X. Y. Ying, Y. Q. Wang, L. G. Wang, W. D. Sheng, A. Wei and Y. Guo, "A stereo attention module for stereo image super-resolution," *IEEE Signal Proc. Let.*, vol. 27, pp. 496–500, 2020. doi: 10.1109/LSP.2020.2973813.

[48] Y. Q. Wang, X. Y. Ying, L. G. Wang, and Y. G. Yang, "Symmetric parallax attention for stereo image super-resolution," in *Proc. Comput. Vis. Pattern Recognit. (CVPR)*, 2021, pp. 766–775.

[49] G. S. Liu, H. J. Yue, Y. Kun, and J. Y. Yang, "Disparity-guided light field image super-resolution via feature modulation and recalibration," *IEEE Trans. Broadcast.*, vol. 69, no. 3, pp. 740–752, 2023. doi: 10.1109/TBC.2023.3284408.

[50] K. Chen, L. Y. Li, H. Liu, Y. Z. Li, C. L. Tang and J. Chen, "SwinFSR: Stereo image super-resolution using SwinIR and frequency domain knowledge," in *Proc. Comput. Vis. Pattern Recognit. (CVPR)*, Vancouver, Canada, 2023, pp. 1764–1774.

[51] Y. Qu, R. K. Baghbaderani, H. Qi, and C. Kwan, "Unsupervised Pansharpening based on self-attention mechanism," *IEEE Trans. Geosci. Remote Sens.*, vol. 59, no. 4, pp. 3192–3208, 2021. doi: 10.1109/TGRS.2020.3009207.

[52] X. Li, H. Y. Zhang, L. P. Zhang, Z. X. Ye, J. T. Pu and M. Yuan, "Swin transformer-based cross-view attention network for stereo image super-resolution," in *Proc. Pattern Recognit. Artif. Intell. (PRAI)*, Haikou, China, 2021, pp. 654–659.

[53] J. Kim, J. K. Lee, and K. M. Lee, "Accurate image super-resolution using very deep convolutional networks," in *Proc. Comput. Vis. Pattern Recognit. (CVPR)*, Las Vegas, NV, USA, 2016, pp. 1646–1654.

[54] Y. L. Zhang, Y. P. Tian, Y. Kong, B. N. Zhong, and Y. Fu, "Residual dense network for image restoration," *Residual Dense Netw. Image Restor.*, vol. 43, no. 7, pp. 2480–2495, 2020. doi: 10.1109/PAMI.2020.2968521.